Grid-connected Self-synchronizing Cascaded H-Bridge Inverters with Autonomous Power Sharing

Soham Dutta*, Minghui Lu*, Branko Majmunovic†, Rahul Mallik*, Gab-Su Seo‡,
Dragan Maksimovic†, and Brian Johnson*

*Department of Electrical and Computer Engineering, University of Washington, Seattle, WA 98195, USA
†Department of Electrical, Computer, and Energy Engineering, University of Colorado, Boulder, CO 80309, USA
‡Power Systems Engineering Center, National Renewable Energy Laboratory, Golden, CO 80401, USA
Corresponding author email: *sdutta@uw.edu*

Abstract—Cascaded inverters are widely applied in applications where elevated ac voltages are required while using semiconductor devices with lower voltage ratings. Here, we focus on structures that require localized power transfer between low-voltage sources/loads dispersed across inverter dc links and the inverter ac-sides are series-connected across a three-phase medium-voltage ac grid. To date, decentralized controllers that allow for bi-directional power transfer in such systems are limited. To fill this gap, we propose a virtual oscillator controller which modulates the power processed by each inverter in a purely decentralized manner. The proposed controller uses only locally measured current, provides communication-free synchronization of the inverter modules, and enables control of power transfer in both directions. Moreover, it is implemented purely in time domain as opposed to phasor-domain based droop controllers. Stability is analyzed and a design procedure for the oscillator parameters is provided alongside relevant simulation and experimental results for a system of five series-connected inverters.

I. INTRODUCTION

Growing demand for highly efficient medium-voltage (MV) grid-connected converters has stimulated innovations in cascaded dc-ac converter topologies. Example applications include ultra-fast electric vehicle chargers and utility-scale solar power plants [1]–[5]. Cascaded structures facilitate the use of low-voltage devices, high voltage gain from dc-input to ac-output side, improved power quality, and a modular system that can accommodate distributed sources/loads on the dc sides. Figure 1 shows such a MV system composed of cascaded H-bridge inverters on the ac-side and isolated bidirectional dc-dc converters on the dc side for interfacing distributed sources or loads and providing isolated dc-links to the downstream inverters.

Focusing on applications where the power processed by each source/load needs to be controlled, existing methods
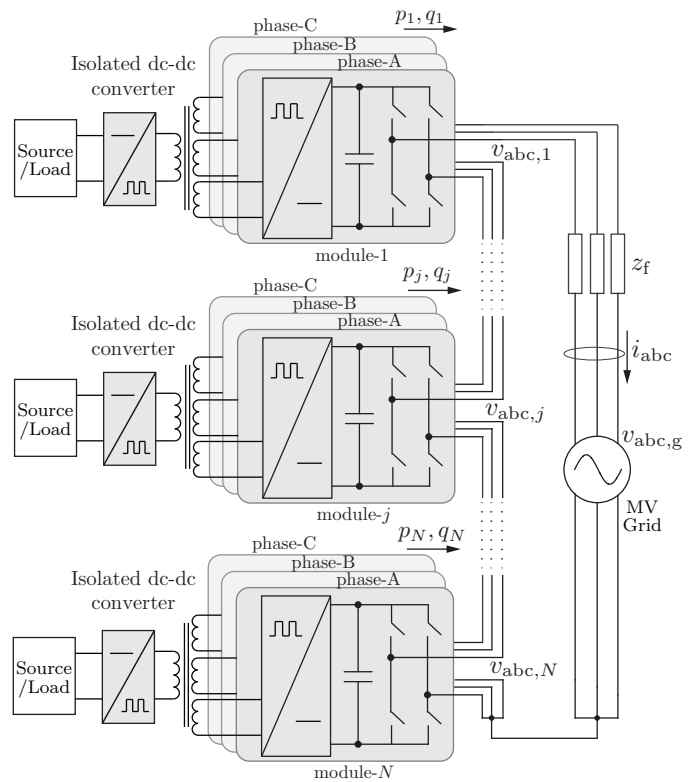

Fig. 1. System where isolated bidirectional dc-dc converters feed cascaded H-bridge inverters across a medium-voltage grid.

typically rely on either a single centralized controller [6]–[8] or distributed controllers with a common communication bus for sending supervisory control commands and grid information [3], [9]–[15]. Centrally-controlled systems not only have a single point of failure, but computational limitations inherent to any control platform act as a bottleneck to system size. Distributed controllers require some form of communication among them which increases wiring complexity and makes high module counts impractical. A common communication bus may also be vulnerable to failure. These issues are collectively overcome by decentralized solutions where each inverter in the stack has its own autonomous controller.

To date, state-of-the-art decentralized control methods have

the following shortcomings which critically affect their usefulness in practical settings. Decentralized methods in [16], [17] are applicable to islanded systems only. Grid connected systems are considered in [18], [19] where each inverter uses an active power versus frequency droop law, but reactive power control is unaddressed and stability only holds for unidirectional power flow. The authors in [20] implemented a decentralized active and reactive power control method for stacked PV inverters where one inverter is controlled in current control mode and the others are voltage controlled. In this setup, the current controlled inverter needs to be of higher transient power rating as the other inverters. Moreover, they still require grid voltage zero-crossing information to be broadcasted, and it should be noted that analysis and experiments are limited to only 3 series-stacked modules. In [21], resistance emulation was introduced in tandem with a modified droop-like controller with both active and reactive power loops. However, the active power controller exhibits instability under reverse power transfer from grid.

To address above mentioned shortcomings, we leverage the intrinsic synchronization and power sharing capabilities of coupled nonlinear Andronov-Hopf oscillators (AHOs) to constitute the decentralized controller of the series-stacked system [22]. The AHO can accept real- and reactive-power setpoints and uses only locally measured current to provide communication-free synchronization and power sharing among the inverter modules. It is applicable to any number of stacked inverter modules and by proper selection of the AHO parameters, we can guarantee control of active power in both directions. Moreover, unlike existing phasor-domain droop-based controllers, our controller is fully executed in time-domain and does not require a power measurement.

The rest of the paper is summarized as follows- Section II provides a detailed model of N series-connected inverters and Section III contains system stability analysis. A parameter selection procedure to ensure stable operation of the controller for both directions of power flow procedure is provided. Finally, relevant simulations and hardware experiments for a prototype with 5 series-stacked converters is provided in Section IV and the paper is concluded in Section V.

II. Dynamical Model of Cascaded H-Bridge Inverter with Virtual Oscillator Controller

Consider the system of N three-phase dc-ac converters connected in series and exchanging power with the utility grid via an impedance z_f as shown in Fig. 1. Each three-phase converter has three single phase H-bridges on its ac output stage. For ease of exposition, we abstract away the dc-side topology and simply show decoupled dc-links although the actual implementation might feature additional upstream circuitry (e.g., dual-active bridges and dc interconnections). We also assume that the dc-link voltages preceding each H-bridge are fixed at a constant value and ignore any dc-side dynamics. Any three-phase vector is represented as $x_{\text{abc}} := [x_a, x_b, x_c]^\top$. The set $\mathcal{N}$ is defined as $\mathcal{N} := \{1, 2, \cdots, N\}$. The converter stack delivers current i_{abc} into the grid. Active and reactive

power processed by the jth converter module is p_j and q_j, respectively, and its instantaneous three-phase terminal voltage is $v_{\text{abc},j}$. We denote the complex filter line impedance as $z_f = R_f + sL_f$. The system current dynamics in the abc frame can then be written as

$$R_f i_{\text{abc}} + L_f \frac{\mathrm{d}i_{\text{abc}}}{\mathrm{d}t} = \sum_{j=1}^{N} v_{\text{abc},j} - v_{\text{abc,g}}. \quad (1)$$

We will express (1) in the dq-frame rotating synchronously at angular velocity ω_{nom} with the d-axis aligned to the grid a-phase voltage. x_{abc} transformed to the $\alpha\beta$ and dq frames is denoted as $x_{\alpha\beta} = [x_\alpha, x_\beta]^\top$ and $x_{dq} = [x_d, x_q]^\top$, respectively. Application of the $abc - dq$ transformation to (1) gives

$$L_f \frac{\mathrm{d}i_d}{\mathrm{d}t} = \sum_{k=1}^{N} v_{d,k} - v_{d,\text{g}} - R_f i_d + \omega_{\text{nom}} L_f i_q, \quad (2)$$

$$L_f \frac{\mathrm{d}i_q}{\mathrm{d}t} = \sum_{k=1}^{N} v_{q,k} - v_{q,\text{g}} - R_f i_q - \omega_{\text{nom}} L_f i_d. \quad (3)$$

A. The Andronov-Hopf Oscillator

The AHO is a nonlinear system that produces sinusoidal oscillations given a nominal amplitude input signal. Its trajectory is adjusted via external active and reactive power setpoints [22]. The state dynamics of the AHO in the absence of setpoints is

$$\begin{bmatrix} \dot{x}_1 \\ \dot{x}_2 \end{bmatrix} = \begin{bmatrix} \xi(2X_{\text{nom}}^2 - \|x\|^2) & -\omega_{\text{nom}} \\ \omega_{\text{nom}} & \xi(2X_{\text{nom}}^2 - \|x\|^2) \end{bmatrix} \begin{bmatrix} x_1 \\ x_2 \end{bmatrix}, \quad (4)$$

where x_1 and x_2 are the states, and X_{nom} is the nominal oscillation RMS amplitude. $\|x\| := (x_1^2 + x_2^2)^{1/2}$ is the Euclidean norm of $[x_1, x_2]^\top$ and the gain ξ influences convergence speed. This is an example of a supercritical Hopf bifurcation where the state trajectories asymptotically spiral towards a stable circular limit cycle with nominal RMS amplitude X_{nom} and angular frequency ω_{nom} from any initial state.

To translate the dynamics in (4) into a hardware-implementable form, we conceptualize the oscillator states as representing the averaged switch-terminal voltages in the in the $\alpha\beta$ and denote them as $[v_{\alpha,j}, v_{\beta,j}]^\top$. The oscillator is then excited by the difference between the commanded line current $[i_\alpha^\star, i_\beta^\star]^\top$ and the actual current $[i_\alpha, i_\beta]^\top$. We get the following voltage dynamics for each inverter:

$$\begin{bmatrix} \dot{v}_{\alpha,j} \\ \dot{v}_{\beta,j} \end{bmatrix} = \begin{bmatrix} k_o\left(2V_{\text{nom}}^2 - \|v_{\alpha\beta}\|^2\right) & -\omega_{\text{nom}} \\ \omega_{\text{nom}} & k_o\left(2V_{\text{nom}}^2 - \|v_{\alpha\beta}\|^2\right) \end{bmatrix} \begin{bmatrix} v_{\alpha,j} \\ v_{\beta,j} \end{bmatrix} - k_f \begin{bmatrix} \cos\phi & -\sin\phi \\ \sin\phi & \cos\phi \end{bmatrix} \begin{bmatrix} i_\alpha - i_\alpha^\star \\ i_\beta - i_\beta^\star \end{bmatrix}, \quad (5)$$

where k_o and k_f are the oscillator convergence and current feedback parameters, respectively. The nonlinear diagonal entries in the voltage dynamics in (5) ensure that the RMS output of each inverter is maintained at V_{nom} with the second term is zero. For grid-connected settings, V_{nom} can be set to the nominal grid RMS voltage $V_{\text{g,nom}}$. Moreover, the parameter ϕ represents a rotation angle that controls the nature of coupling between the current and the voltage of a particular axis.
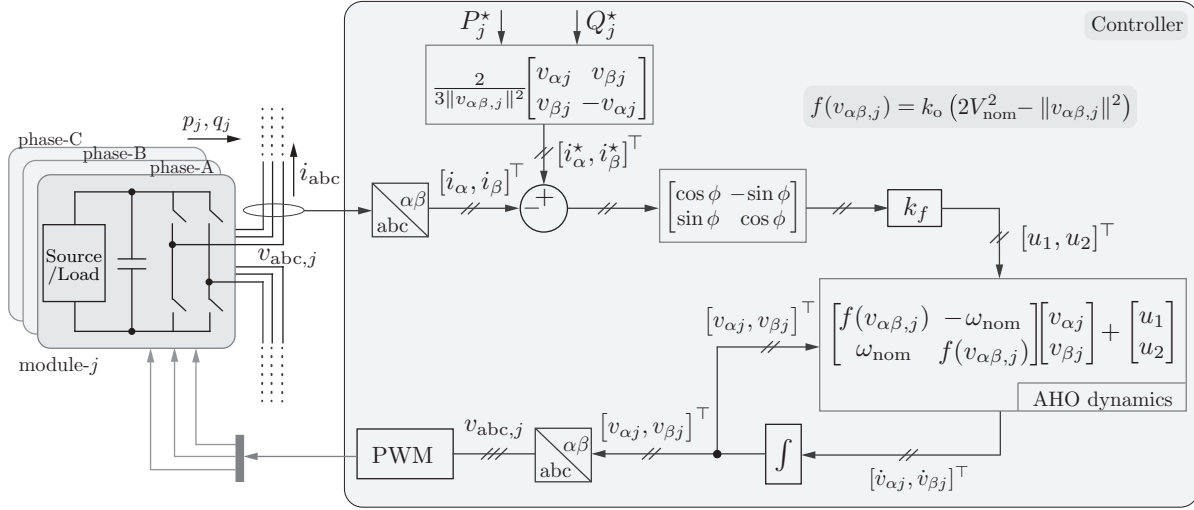
2807

Fig. 2. A cascaded inverter module with the proposed nonlinear oscillator-based controller.

Current references at the jth inverter are given by

$$i_{\alpha,j}^{\star} = \frac{2}{3} \frac{v_{\alpha,j} P_j^{\star} + v_{\beta,j} Q_j^{\star}}{\|v_{\alpha\beta,j}\|^2}, \; i_{\beta,j}^{\star} = \frac{2}{3} \frac{v_{\beta,j} P_j^{\star} - v_{\alpha,j} Q_j^{\star}}{\|v_{\alpha\beta,j}\|^2}. \quad (6)$$

Substituting (6) into (5) and transforming the dynamics in (5) into the synchronous dq frame gives (7)–(8). For ease of exposition, we use (9)–(10) to obtain the following voltage amplitude and angular dynamics

$$\dot{V}_j = \frac{v_{d,j}\dot{v}_{d,j} + v_{q,j}\dot{v}_{q,j}}{\|v_{dq,j}\|} = k_{\text{o}}(2V_{\text{nom}}^2 - V_j^2)V_j$$
$$+ \frac{2k_f}{3V_j}\left(\cos\phi(P_j^{\star} - p_j) + \sin\phi(Q_j^{\star} - q_j)\right), \quad (9)$$

$$\dot{\theta}_j = \arctan\left(\frac{v_{q,j}}{v_{d,j}}\right)$$
$$= \frac{2k_f}{3V_j^2}\left(\sin\phi(P_j^{\star} - p_j) - \cos\phi(Q_j^{\star} - q_j)\right), \quad (10)$$

where V_j is the jth voltage amplitude and θ_j is the voltage phase angle with respect to the d-axis or grid phase-a voltage. The implementation of this controller is shown in Fig. 2.

B. Steady-state solutions

Setting derivatives in (9)-(10) to zero, the steady-state voltage amplitude and power values can be expressed as

$$V_j = V_{\text{nom}}\left(1 \pm \sqrt{1 + \frac{k_f f(\phi)}{3k_{\text{o}}V_{\text{nom}}^4}}\right)^{\frac{1}{2}}, \quad (11)$$

$$\sin(\phi)(P_j^{\star} - P_j) - \cos(\phi)(Q_j^{\star} - Q_j) = 0, \quad (12)$$

where

$$f(\phi) = \begin{cases} (P_j^{\star} - P_j)/\cos\phi, & \text{if } \phi \neq \pi/2 \\ (Q_j^{\star} - Q_j)/\sin\phi, & \text{if } \phi \neq 0 \end{cases}. \quad (13)$$

Above, P_j and Q_j are the steady-state values of active and reactive power, respectively. Therefore, we can see that depending on the selection of ϕ various modes of coupling between V_j and P_j or Q_j can be obtained. In (12), it is evident that ideal tracking of reactive power (i.e., $Q_j = Q_j^{\star}$) and real power (i.e., $P_j = P_j^{\star}$) follow when $\phi = 0$ and $\phi = \pi/2$, respectively. The steady-state voltage amplitude, phase angle, active power error, and reactive power error with variations in $P_j^{\star}$ are in Fig. 3 with parameters in Table I.

III. STABILITY ANALYSIS AND PARAMETER SELECTION

To assess stability, we contain the dq grid currents as well as all inverter voltage amplitudes and phase angles within the state vector, $x = [V_1, \theta_1, \cdots, V_N, \theta_N, i_d, i_q]^{\top}$ of length $2(N+1)$. The nonlinear state equations are summarized in (2)–(3) and (14)–(15) $\forall j \in \mathcal{N}$. Now we evaluate the steady state condition where all active power setpoints are equal and reactive power setpoints are zero. Hence, $P_j^{\star} = P^{\star}$ and $Q_j^{\star} = Q^{\star} = 0$, $\forall j \in \mathcal{N}$. In this condition, the steady-state voltage amplitudes and angles are equal such that $V_j = V_{\text{o}}$ and $\theta_j = \theta_{\text{o}}$, $\forall j \in \mathcal{N}$. Linearizing around this equilibrium

$$\frac{dv_{d,j}}{dt} = k_{\text{o}}\left(2V_{\text{nom}}^2 - \|v_{dq,j}\|^2\right)v_{d,j} - k_f\left(i_d\cos\phi - \frac{2\cos\phi}{3\|v_{dq,j}\|^2}\left(P_j^{\star}v_{d,j} + Q_j^{\star}v_{q,j}\right) - i_q\sin\phi + \frac{2\sin\phi}{3\|v_{dq,j}\|^2}\left(P_j^{\star}v_{q,j} - Q_j^{\star}v_{d,j}\right)\right),$$
$$\quad (7)$$

$$\frac{dv_{q,j}}{dt} = k_{\text{o}}\left(2V_{\text{nom}}^2 - \|v_{dq,j}\|^2\right)v_{q,j} - k_f\left(i_d\sin\phi - \frac{2\sin\phi}{3\|v_{dq,j}\|^2}\left(P_j^{\star}v_{d,j} + Q_j^{\star}v_{q,j}\right) + i_q\cos\phi - \frac{2\cos\phi}{3\|v_{dq,j}\|^2}\left(P_j^{\star}v_{q,j} - Q_j^{\star}v_{d,j}\right)\right).$$
$$\quad (8)$$

2808

$$\frac{\mathrm{d}V_j}{\mathrm{d}t} = k_\mathrm{o}\left(2V_\mathrm{nom}^2 - V_j^2\right)V_j + \cos\phi\left(\frac{2k_f}{3V_j}P_j^\star - k_f\left(\cos\theta_j i_d + \sin\theta_j i_q\right)\right) + \sin\phi\left(\frac{2k_f}{3V_j}Q_j^\star - k_f\left(\sin\theta_j i_d - \cos\theta_j i_q\right)\right),$$
(14)

$$\frac{\mathrm{d}\theta_j}{\mathrm{d}t} = \sin\phi\left(\frac{2k_f}{3V_j^2}P_j^\star - \frac{k_f}{V_j}\left(\cos\theta_j i_d + \sin\theta_j i_q\right)\right) - \cos\phi\left(\frac{2k_f}{3V_j^2}Q_j^\star - \frac{k_f}{V_j}\left(\sin\theta_j i_d - \cos\theta_j i_q\right)\right).$$
(15)

yields the Jacobian matrix:

$$\mathbf{J} = \begin{bmatrix} \alpha & \alpha' & \cdots & 0 & 0 & \kappa_1 & \kappa_2 \\ \beta' & \beta & \cdots & 0 & 0 & -\frac{\kappa_2}{V_\mathrm{o}} & \frac{\kappa_1}{V_\mathrm{o}} \\ \vdots & \vdots & \ddots & \vdots & \vdots & \vdots & \vdots \\ 0 & 0 & \cdots & \alpha & \alpha' & \kappa_1 & \kappa_2 \\ 0 & 0 & \cdots & \beta' & \beta & -\frac{\kappa_2}{V_\mathrm{o}} & \frac{\kappa_1}{V_\mathrm{o}} \\ c_1 & -V_\mathrm{o}c_2 & \cdots & c_1 & -V_\mathrm{o}c_2 & -\frac{R_\mathrm{f}}{L_\mathrm{f}} & \omega_\mathrm{nom} \\ c_2 & V_\mathrm{o}c_1 & \cdots & c_2 & V_\mathrm{o}c_1 & -\omega_\mathrm{nom} & -\frac{R_\mathrm{f}}{L_\mathrm{f}} \end{bmatrix}.$$
(16)

The expressions for $\alpha, \alpha', \beta, \beta', \kappa_1, \kappa_2, c_1,$ and c_2 are given in the Appendix. This matrix can be written in the form

$$\mathrm{J} = \begin{bmatrix} \mathbf{A} & \cdots & \mathbf{0} & \mathbf{B} \\ \vdots & \ddots & \vdots & \vdots \\ \mathbf{0} & \cdots & \mathbf{A} & \mathbf{B} \\ \mathbf{C} & \cdots & \mathbf{C} & \mathbf{Z} \end{bmatrix},$$
(17)

where

$$\mathbf{A} = \begin{bmatrix} \alpha & \alpha' \\ \beta' & \beta \end{bmatrix}, \quad \mathbf{B} = \begin{bmatrix} \kappa_1 & \kappa_2 \\ -\frac{\kappa_2}{V_\mathrm{o}} & \frac{\kappa_1}{V_\mathrm{o}} \end{bmatrix},$$

$$\mathbf{C} = \begin{bmatrix} c_1 & -V_\mathrm{o}c_2 \\ c_2 & V_\mathrm{o}c_1 \end{bmatrix}, \quad \mathbf{Z} = \begin{bmatrix} -\frac{R_\mathrm{f}}{L_\mathrm{f}} & \omega_\mathrm{nom} \\ -\omega_\mathrm{nom} & -\frac{R_\mathrm{f}}{L_\mathrm{f}} \end{bmatrix},$$

and $\mathbf{0}$ is a 2×2 matrix of all zeros. The characteristic equation of this matrix form is

$$|\lambda\mathbf{I} - \mathbf{A}|^{N-1}|(\lambda\mathbf{I} - \mathbf{A})(\lambda\mathbf{I} - \mathbf{Z}) - N\mathbf{CB}| = 0,$$
(18)

where $|.|$ denotes the matrix determinant and $\mathbf{I}$ is a 2×2 identity matrix.

A. Eigenvalue Analysis

Solving (18) gives a total of $2(N + 1)$ eigenvalues, out of which $2(N - 1)$ are conjugate pairs of the form

$$\lambda_{1,1'} = 0.5(\alpha + \beta) \pm 0.5\left((\alpha - \beta)^2 + 4\alpha'\beta'\right)^{\frac{1}{2}},$$
(19)

with multiplicity $N - 1$. For $\phi = \pi/2$, λ_1 and $\lambda_{1'}$ can be simplified as

$$\lambda_1 = (\alpha + \beta) + \frac{\alpha'\beta' - \alpha\beta}{\alpha + \beta} \approx (\alpha + \beta)$$

$$\approx -4k_\mathrm{o}V_\mathrm{nom}^2 < 0, \quad \text{if } k_\mathrm{o} > 0,$$
(20)

$$\lambda_{1'} = -\frac{\alpha'\beta' - \alpha\beta}{\alpha + \beta} \approx \frac{k_f Q}{3V_\mathrm{nom}^2}, \quad \text{when } \phi = \frac{\pi}{2}.$$
(21)

When $\phi = 0$, (27)-(28) imply $\alpha' \approx 0$, $\beta' \approx 0$. Hence,

$$\lambda_1 \approx \alpha \approx -4k_\mathrm{o}V_\mathrm{nom}^2 - \frac{k_f P^\star}{3V_\mathrm{nom}^2},$$
(22)

$$\lambda_{1'} \approx \beta \approx \frac{k_f P}{3V_\mathrm{nom}^2}, \quad \text{when } \phi = 0.$$
(23)

Recall that P and Q are the values of active and reactive power, respectively, delivered by each inverter in steady state. When $\phi = \pi/2$ and $Q < 0$, then $\lambda_1' < 0$. For this mode of coupling Q is not tightly controlled and the oscillator adjusts the inverter voltage amplitudes such that, $Q < 0$ in steady state and the system is stable. However, in the case of power transfer from the grid to the inverters, $P < 0$ and, hence, we need $Q > 0$ for stability. In that case, the system becomes unstable if $\phi = \pi/2$ is still maintained. Therefore, for reverse power transfer it follows that we must select the mode of coupling where $\phi = 0$ so that $\lambda_1' < 0$ as $P < 0$.
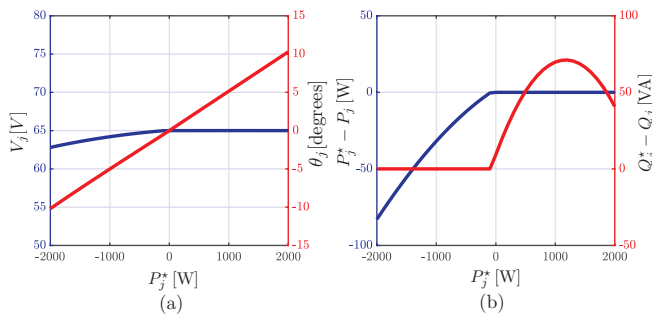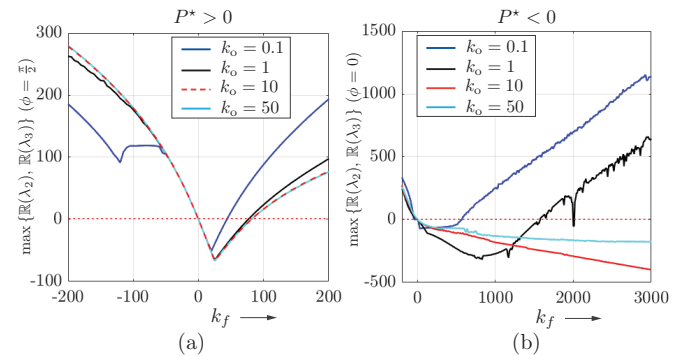

Fig. 3. Plot of steady-state quantities with active power reference variation: (a) steady-state voltage amplitude and phase angle, (b) steady-state active power error and reactive power error.

Fig. 4. Plot showing trajectories of real-parts of critical eigenvalues λ_2 and λ_3 as a function of k_f for different values of k_o in case of, (a) forward power transfer, (b) reverse power transfer.

The remaining 4 eigenvalues of $\mathbf{J}$ come in conjugate pairs, and are solutions of the following matrix equation:

$$|(\lambda I - \mathbf{A})(\lambda I - \mathbf{Z}) - N\mathbf{CB}| = 0. \quad (24)$$

The solutions of (24) are denoted as $\lambda_{2,2'}$ and $\lambda_{3,3'}$, which have 2 distinct real parts $\mathbb{R}(\lambda_2)$ and $\mathbb{R}(\lambda_3)$, respectively. Figure 4 shows the plot of the maximum of these two real parts as a function of the oscillator parameter k_o and feedback gain k_f. As illustrated in Fig. 4, there exists a range of k_f and k_o that ensure $\max\{\mathbb{R}(\lambda_2), \mathbb{R}(\lambda_3)\} < 0$. Based on this, we select k_f and k_o appropriately for both $P^\star > 0$ and $P^\star < 0$. The chosen values used in the upcoming experiments are in Table II.

IV. SIMULATION AND EXPERIMENTAL RESULTS

The numerical simulations and hardware experiments in this section substantiate the preceding design approach and supporting analysis. The scaled down version has 5 dc-ac converters connected in series and the system and controller parameters for each purpose are given in Table-I and Table-II.

A. Simulation Results

Our simulation captures the dynamics of five cascaded H-bridges with ideal dc voltage source inputs. The system and controller under consideration are in Table-I. System performance for negative active power transfer is shown in Fig. 5. Figure 5(a) exemplifies communication-free synchronization

Symbol	Description	Value	Units
$V_{g,nom}$	Nominal grid voltage	230	V_{rms}
ω_{nom}	Nominal grid frequency	60	Hz
V_{dc}	Dc-link voltage	50	V
f_{nom}	Inverter switching frequency	10	kHz
L_f	Filter inductance	5	mH
R_f	Filter resistance	0.2	Ω
V_{nom}	Nominal oscillator amplitude	46	V_{rms}

among the oscillator-controlled inverters and Fig. 5(b) illustrates active power reference tracking when every $10\,ms$ each inverter is issued a distinct $-1\,kW$ step command. Reactive power dynamics are in Fig. 5(c) with fixed $0\,VAR$ references and Fig. 5(d) confirms near unity power factor operation. Next, Fig. 6(a)–(d) provide similar results for active power delivery from the inverter stack to the grid.

B. Experimental Results

Our three-phase hardware system, as depicted in Fig. 7, has five series-connected H-bridge inverters for ac phase leg. Looking further upstream, the system topology mirrors that in Fig. 1 where each dc-link is interfaced by a dual active bridge (DAB) which are in turn powered by a single dc power supply. Each DAB stage provides isolation to facilitate
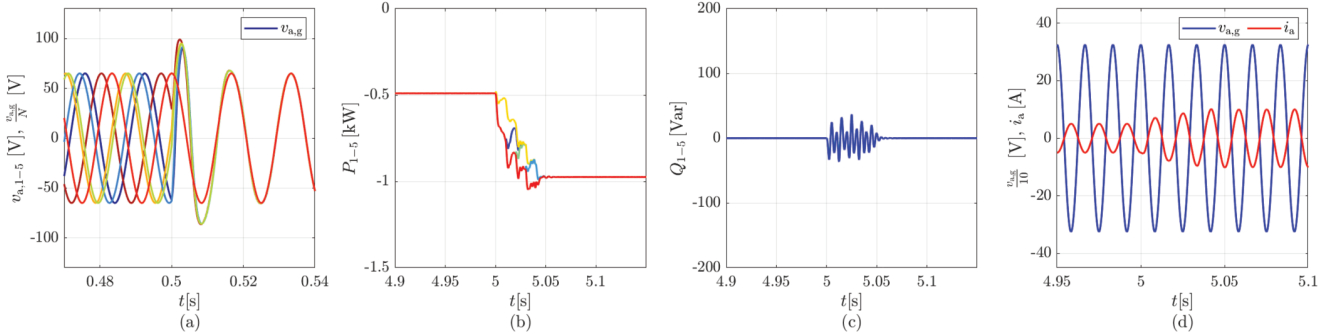

Fig. 5. Simulation results for negative active power transfer with $\phi = 0$, $k_o = 1$, and $k_f = 1000$). (a) Communication-free voltage synchronization, (b) Active power reference tracking, (c) Reactive power output, (d) Near-unity-power-factor operation of output voltage and grid current.
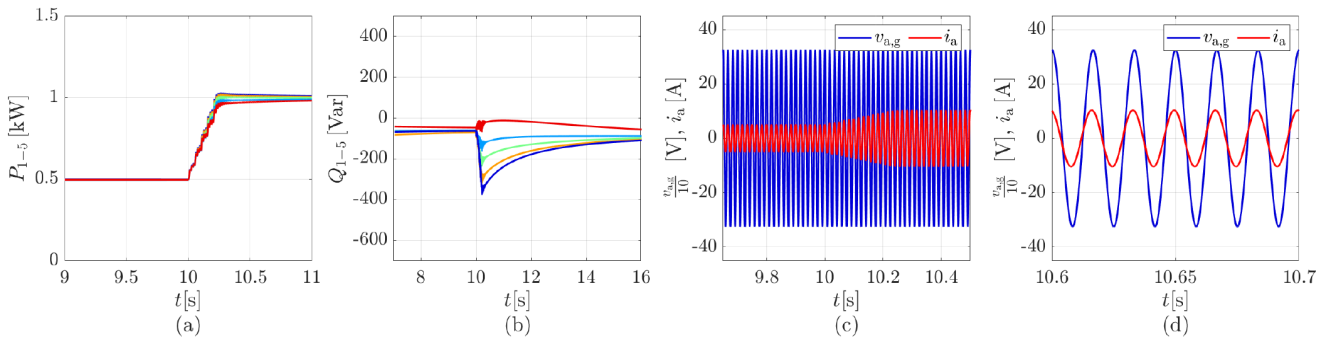

Fig. 6. Simulation results for positive active power delivery $\phi = \pi/2$, $k_o = 0.1$, and $k_f = 20$. (a) Active power reference tracking, (b) Reactive power output, (c) Grid current response to power step change, (d) In-phase output voltage and grid current.

Symbol	Description	Value	Units
V_{in}	DAB input voltage	100	V
n	DAB transformer turns ratio	2:1	
V_{dc}	Dc-link voltage	50	V
$V_{\text{g,nom}}$	Nominal grid voltage	106	V_{rms}
ω_{nom}	Nominal grid frequency	60	Hz
f_{nom}	HBI switching frequency	10	kHz
L_{f}	Filter inductance	5	mH
R_{f}	Filter resistance	0.25	Ω
V_{nom}	Nominal oscillator amplitude	21.2	V_{rms}
	Case-I: Forward power transfer		
ϕ	Current rotation angle	$\pi/2$	rad
k_f	Current feedback gain	20	Ω/s
k_{o}	AHO convergence parameter	1	$1/(V^2 s)$
	Case-II: Reverse power transfer		
ϕ	Current rotation angle	0	rad
k_f	Current feedback gain	1000	Ω/s
k_{o}	AHO convergence parameter	1	$1/(V^2 s)$

ac-side stacking. Finally, each set of three-phase H-bridges has local current sensing circuitry and is digitally controlled by a TMS320F28379D digital signal processor. Hence, there are a total of five decentralized digital controllers. These digital controllers also modulate the DABs to provide voltage regulation for each three-phase set of floating dc-links. The experimentally used physical and control parameters are in Table II.

1) Pre-synchronization with grid: In order to pre-synchronize the inverters with the grid, the active and reactive

Fig. 8. Experimental validation of forward power transfer: Transient response when $P^\star$ changes from 10 W to 100 W at each inverter. Grid voltages and currents are depicted.

power set-points for each converter are set to 0 and a resistance is introduced into the circuit to limit the grid current as the inverter voltages build up. In this condition, the oscillator-based controller exactly tracks the grid voltage and the current decays to zero. This is when the startup resistance is removed and the inverters can begin delivering power into the grid.

2) Forward power transfer: Figure 8 shows the transient response of the system when all of the inverter units are given a step change in the active power command from $P^\star = 10$ W to $P^\star = 100$ W. The total active power delivery is close to $P_{\text{grid}} = 500$ W. Similarly, Fig. 9 shows the transient response as well as the steady-state waveforms of the system when all of the inverter units are given a power command step change from $P^\star = 100$ W to $P^\star = 200$ W. The reactive power set-point is
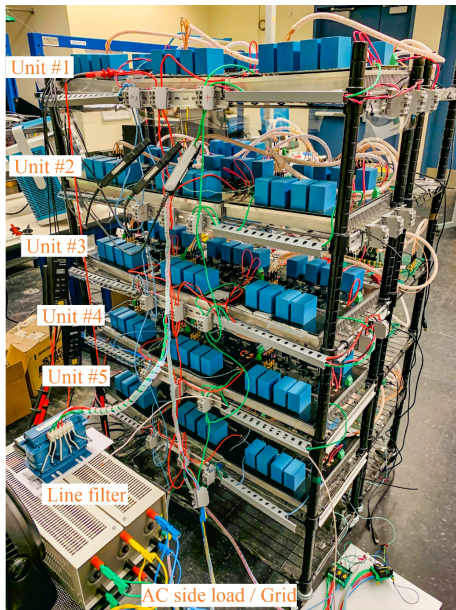

Fig. 7. Experimental setup consisting of five cascaded three-phase dc-ac converter units. Each unit consists of three DABs and three H-bridges.
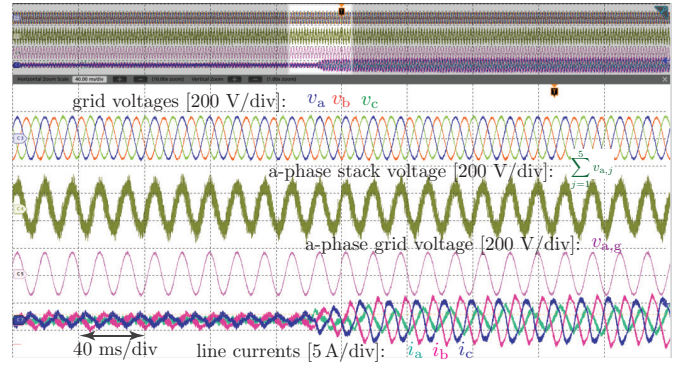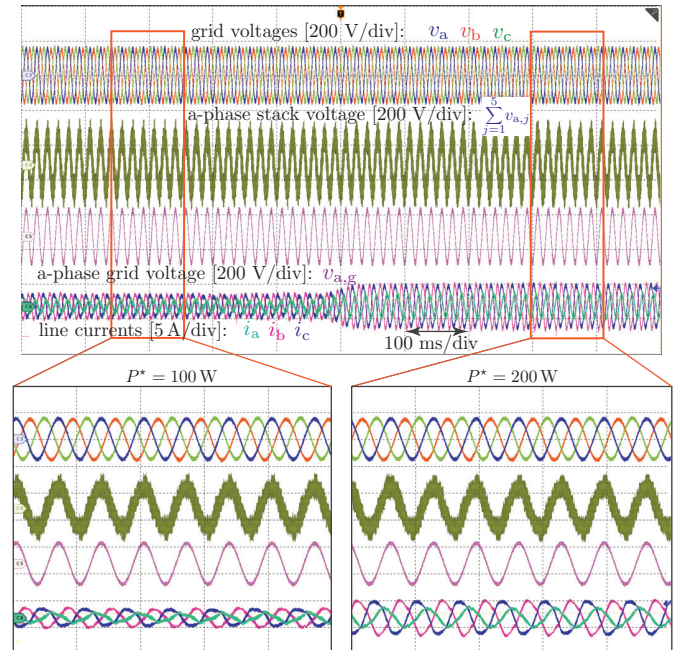

Fig. 9. Forward power transfer: Transient response when $P^\star$ changes from 100 W to 200 W at each inverter.

2811

Fig. 10. Transient response of dc-supply currents at DAB inputs during a $P^\star$ step-change from $100\,\mathrm{W}$ to $200\,\mathrm{W}$. Inverters equally share grid reactive power.

kept at $Q^\star = 0$. The total active power delivered to the grid in this case is close to $P_\mathrm{grid} = 1\,\mathrm{kW}$. Since reactive power is not tightly regulated, some small amount of reactive power is absorbed from the grid. Note that the three-phase currents are not equal because of the presence of small imbalances among the converters and lack of sensor calibration. Such issues could be mitigated in a commercial environment. Figure 10 shows the dc supply input currents of the five units for a $100\,\mathrm{W}$ to $200\,\mathrm{W}$ power command step . It can be seen that the average dc current for all the modules changes from $1\,\mathrm{A}$ to $2\,\mathrm{A}$ as the power increases.

3) Reverse power transfer: Experimental results in Fig. 11 are for the case of reverse power transfer from grid to the converters. Here, the active power reference is changed from $P^\star = -50\,\mathrm{W}$ to $P^\star = -100\,\mathrm{W}$ while keeping $Q^\star = 0$. Since, the voltage amplitude governs the active power flow in this scenario, the line currents have distortion due to the multilevel voltage waveform. This distortion could be damped out via digital resistance emulation. This will be considered in future work. Due to the coupling between frequency and reactive power, the reactive power is perfectly controlled at $0\,\mathrm{VAR}$ whereas the active power has some error.

Fig. 11. Measurements during reverse power transfer: Transient response when $P^\star$ is adjusted from $-50\,\mathrm{W}$ to $-100\,\mathrm{W}$ at each inverter.

V. Conclusion

This outlines a decentralized control method for grid-connected cascaded H-bridge inverters. We envision this approaching as having applications in transformerless medium-voltage converters. In the proposed framework, cascaded dc-ac converters autonomously regulate their active and reactive power output using a virtual oscillator controller. our controller provides communication-free synchronization and power sharing among the cascaded units and its time domain implementation gives speed advantages over conventional phasor-based droop methods. Unlike prior methods, this method can control the active power processed by an inverter in both directions and can be applied to any number of series-connected converters. To formulate an analytical foundation, the nonlinear system model was first provided and the eigenvalues of its linearized counterpart were subsequently computed. The analytical expressions of the eigenvalues guided parameter selection with the aim of guaranteeing small-signal stability during both positive and negative power transfer. Finally, experimental measurements were shown for a system of five series-connected three-phase dc-ac modules.

Appendix

The expressions for matrix entries in (16) are

$$\alpha = k_\mathrm{o}\left(2V_\mathrm{nom}^2 - 3V_\mathrm{o}^2\right) - \frac{2k_f}{3V_\mathrm{o}^2}\left(P^\star \cos\phi + Q^\star \sin\phi\right), \tag{25}$$

$$\beta \approx \frac{2k_f}{3V_\mathrm{o}^2}\left(P\cos\phi + Q\sin\phi\right), \tag{26}$$

$$\alpha' \approx -\frac{2k_f}{3V_\mathrm{o}}\left(P\sin\phi - Q\cos\phi\right), \tag{27}$$

$$\beta' \approx -\frac{2k_f}{3V_\mathrm{o}^3}\left(Q\cos\phi + P\sin\phi\right), \tag{28}$$

$$\kappa_1 = -k_f\cos\left(\theta_\mathrm{o} - \phi\right), \quad \kappa_2 = -k_f\sin\left(\theta_\mathrm{o} - \phi\right), \tag{29}$$

$$c_1 = \cos\theta_\mathrm{o}/L_\mathrm{f}, \quad c_2 = \sin\theta_\mathrm{o}/L_\mathrm{f}. \tag{30}$$

References

[1] S. Inoue and H. Akagi, "A bidirectional isolated DC-DC converter as a core circuit of the next-generation medium-voltage power conversion system," *IEEE Trans. Power Electron.*, vol. 22, no. 2, pp. 535–542, 2007.

[2] S. Srdic and S. Lukic, "Toward extreme fast charging: Challenges and opportunities in directly connecting to medium-voltage line," *IEEE Electrif. Mag.*, vol. 7, no. 1, pp. 22–31, 2019.

[3] P. K. Achanta, B. B. Johnson, G.-S. Seo, and D. Maksimovic, "A multilevel DC to three-phase AC architecture for photovoltaic power plants," *IEEE Trans. Energy Convers.*, vol. 34, no. 1, pp. 181–190, 2018.

[4] S. Essakiappan, H. S. Krishnamoorthy, P. Enjeti, R. S. Balog, and S. Ahmed, "Multilevel medium-frequency link inverter for utility scale photovoltaic integration," *IEEE Trans. Power Electron.*, vol. 30, no. 7, pp. 3674–3684, 2014.

[5] D. Sha, G. Xu, and Y. Xu, "Utility direct interfaced charger/discharger employing unified voltage balance control for cascaded H-bridge units and decentralized control for cf-dab modules," *IEEE Trans. Ind. Electron.*, vol. 64, no. 10, pp. 7831–7841, 2017.

[6] A. Dell'Aquila, M. Liserre, V. G. Monopoli, and P. Rotondo, "Overview of PI-based solutions for the control of DC buses of a single-phase H-bridge multilevel active rectifier," *IEEE Trans. Ind Appl.*, vol. 44, no. 3, pp. 857–866, 2008.
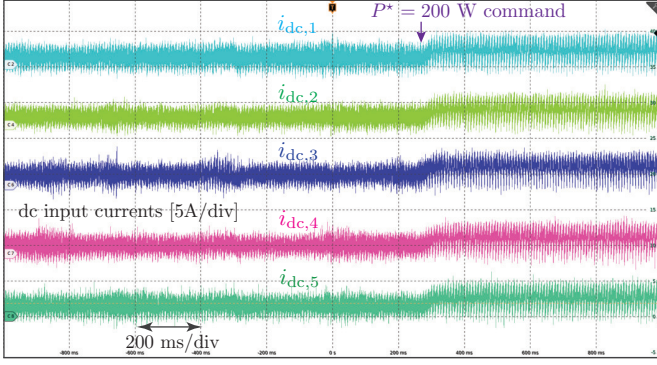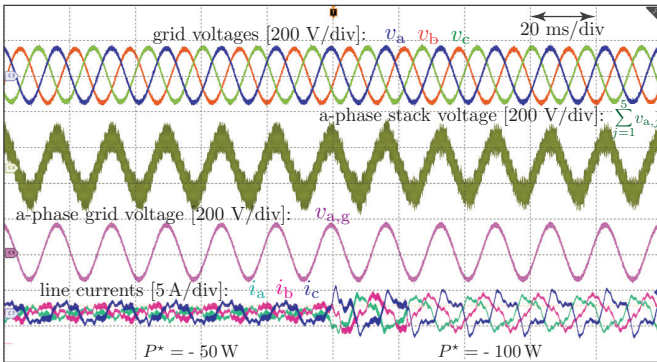
[7] E. Villanueva, P. Correa, J. Rodríguez, and M. Pacas, "Control of a single-phase cascaded h-bridge multilevel inverter for grid-connected photovoltaic systems," *IEEE Trans. Ind. Electron.*, vol. 56, no. 11, pp. 4399–4406, 2009.

[8] T. Zhao, G. Wang, S. Bhattacharya, and A. Q. Huang, "Voltage and power balance control for a cascaded H-bridge converter-based solid-state transformer," *IEEE Trans. Power Electron.*, vol. 28, no. 4, pp. 1523–1532, 2012.

[9] B. P. McGrath, D. G. Holmes, and W. Y. Kong, "A decentralized controller architecture for a cascaded H-bridge multilevel converter," *IEEE Trans. Ind. Electron.*, vol. 61, no. 3, pp. 1169–1178, 2013.

[10] L. Zhang, K. Sun, Y. W. Li, X. Lu, and J. Zhao, "A distributed power control of series-connected module-integrated inverters for pv grid-tied applications," *IEEE Trans. Power Electron.*, vol. 33, no. 9, pp. 7698–7707, 2017.

[11] P. K. Achanta, D. Maksimovic, and M. Ilic, "Decentralized control of series stacked bidirectional DC-AC modules," in *2018 IEEE Applied Power Electronics Conference and Exposition*, pp. 1008–1013, 2018.

[12] J. He, Y. Li, C. Wang, Y. Pan, C. Zhang, and X. Xing, "Hybrid microgrid with parallel-and series-connected microconverters," *IEEE Trans. Power Electron.*, vol. 33, no. 6, pp. 4817–4831, 2017.

[13] H. Jafarian, S. Bhowmik, and B. Parkhideh, "Hybrid current-/voltage-mode control scheme for distributed ac-stacked PV inverter with low-bandwidth communication requirements," *IEEE Trans. Ind. Electron.*, vol. 65, no. 1, pp. 321–330, 2017.

[14] B. Xu, H. Tu, Y. Du, H. Yu, H. Liang, and S. Lukic, "A distributed control architecture for cascaded H-bridge converter with integrated battery energy storage," *IEEE Trans. Ind Appl.*, vol. 57, no. 1, pp. 845–856, 2020.

[15] X. Hou, K. Sun, X. G. Zhang, Y. Sun, and J. Lu, "A hybrid volt-age/current control scheme with low-communication burden for grid-connected series-type inverters in decentralised manner," *IEEE Trans. Power Electron.*, 2021.

[16] J. He, Y. Li, B. Liang, and C. Wang, "Inverse power factor droop control for decentralized power sharing in series-connected-microconverters-based islanding microgrids," *IEEE Trans. Ind. Electron.*, vol. 64, no. 9, pp. 7444–7454, 2017.

[17] P. Achanta, M. Sinha, B. Johnson, S. Dhople, and D. Maksimovic, "Self-synchronizing series-connected inverters," in *Workshop on Control and Modeling for Power Electronics*, pp. 1–6, 2018.

[18] X. Hou, Y. Sun, X. Zhang, G. Zhang, J. Lu, and F. Blaabjerg, "A self-synchronized decentralized control for series-connected H-bridge rectifiers," *IEEE Trans. Power Electron.*, vol. 34, no. 8, pp. 7136–7142, 2019.

[19] X. Hou, Y. Sun, H. Han, Z. Liu, W. Yuan, and M. Su, "A fully decentralized control of grid-connected cascaded inverters," *IEEE Trans. Sustain. Energy*, vol. 10, no. 1, pp. 315–317, 2018.

[20] H. Jafarian, R. Cox, J. H. Enslin, S. Bhowmik, and B. Parkhideh, "Decentralized active and reactive power control for an AC-stacked PV inverter with single member phase compensation," *IEEE Trans. Ind Appl.*, vol. 54, no. 1, pp. 345–355, 2017.

[21] S. Dutta, M. Lu, R. Mallik, B. Majmunovic, S. Mukherjee, G.-S. Seo, D. Maksimovic, and B. Johnson, "Decentralized control of cascaded H-bridge inverters for medium-voltage grid integration," in *2020 IEEE 21st Workshop on Control and Modeling for Power Electronics*, pp. 1–6, 2020.

[22] M. Lu, S. Dutta, V. Purba, S. Dhople, and B. Johnson, "A grid-compatible virtual oscillator controller: Analysis and design," in *2019 IEEE Energy Conversion Congress and Exposition*, pp. 2643–2649, 2019.